China Steel Technical Report, No. 21, pp. 1 −6, (2008)

Investigations of Microstructure and Phosphorus Distribution in BOF Slag

KU-LING CHANG, CHU-TAUR HUANG, WIN- JAY HUANG and YUANG-CHANG LIU

Steel and Aluminum Research and Development Department
China Steel Corporation
Hsiao Kang, Kaohsiung 81233, Taiwan, R.O.C.

Efficient slag-making is a key process to improve the dephosphorization capability in the BOF operation. The microstructure analyses can provide the complete information of phosphorus distribution in the various mineral phases to feature in the dephosphorization process. The characteristics of high basicity BOF slag had been reported widely. However, the investigations on the low basicity slag properties for dephosphorization in BOF are rarely discussed in the steelmaking slag system. Two kinds of BOF slag, conventional slag with high basicity and dephosphorization slag with low basicity, were investigated in this study focusing on the microstructure and phosphorus-containing phases analysis. The slag composition and the mineral phase were examined by XRF chemical analysis, EPMA and XRD studies. The results indicated that the phosphorus-containing phase in high basicity slag was the dicalcium silicate ($2CaO{\cdot}SiO_2$ or C_2S) phase, while phosphorus in low basicity slag was incorporated in a $CaFeSiO_4$ structure.

1. INTRODUCTION

The composition of the mineral phases can be characterized by slag microstructure analysis. A slag structure composed of different mineral phases is associated with the slagging performance through its chemical and physical properties. In contrast to the formal chemical composition analysis, the combination of the mineral phase, the chemical composition, and the melting point of the slag can explain the behavior characteristics of slag comprehensively. Therefore, the mineral phase is an important reference in the slagging practice for dephosphorization in the BOF process.

Some pretreatment and refining technologies have been developed to advance the BOF operation for dephosphorization. Yuji Ogawa et al (1) reported that the MURC (Multi-Refining Converter) process using an 8-ton experimental furnace could enhance the efficiency of dephosphorization. This process consisted of continuous dephosphorization and decarburization continuously in the same furnace with intermediate deslagging followed by dephosphorization and/or desiliconization simultaneously. A slag with a lower melting point was required because good fluidity was essential to increase the deslagging ability. Consequently, the dephosphorization slag was designed with low basicity (CaO/SiO_2=1~1.8), which was apparently distinct to conventional BOF process.

Several mineral phases in conventional BOF slag have been examined,(2-3) such as dicalcium silicate (C_2S), tricalcium silicate, wustite, magnesio-wustite, calcium ferrite and lime. The formation of these mineral phases in slag was dependent on the slagging practice. In comparison with conventional BOF slag (CaO/SiO_2=3~4), the mineralogical morphology investigations into the low basicity slag for dephosphorization are scarce in steelmaking slag system. The objective of this study focused on the microstructure of conventional BOF slag and dephosphorization slag with low basicity.

2. EXPERIMENTAL METHOD

All slag samples were taken from the BOF in the steelmaking plant. Two stages practice were considered during BOF operation, dephosphorization and decarburization. The slag samples with high basicity were taken at end of blowing (2nd stage), while with low basicity samples were taken at deslagging followed by dephosphorization (1st stage). The slag composition and mineral phase were examined and the X-ray fluorescence (XRF) chemical analysis and Electron Probe Micro Analyzer (EPMA), XRD performed. For the XRD measurements, the slag specimens were analyzed using $\theta/2\theta$ diffraction mode ranging from 10° to 70°.

The concentration of each element in the samples was analyzed by the wave length dispersion type EPMA. The percentages of all elements were given as oxides (wt%), which were calculated stoichiometrically from element (wt%) data results. A total iron (T-Fe) was designated since the iron might be present in different oxidation states. Each element was set to a constant input value due to the stoichiometry. The EPMA analysis of iron was assumed to be bound as FeO in this study.

3. RESULTS AND DISCUSSION

The chemical compositions of the BOF slag selected for mineral phase analysis are listed in Table 1, where H1 and H2 are slags with high basicity, and L1-L4 slags with low basicity.

The components of SiO_2 and T-Fe in the low basicity slags are higher than those in the high basicity slags. However, the component of CaO in low basicity slag is lower as compared with high basicity.

3.1 XRD Analysis

The X-ray diffraction patterns of high basicity slag (H1 and H2) are shown in Fig. 1, where the mineral phases of dicalcium silicate, calcium ferrite and wustite are identified. The presence of dicalcium silicate (C_2S) is the preferred phase in slag from the observed peak intensity, which shows that the C_2S phase is the main constituent in high basicity BOF slag. Figure 2 and Fig. 3 illustrate respectively the X-ray diffraction patterns for the low basicity slags L1, L2 and L3, L4. The obviously differences in the XRD spectra can be distinctly observed in comparison with the spectra of high basicity slag in Fig. 1. In Fig. 2 and Fig. 3, a different diffraction peaks in the range of 2θ : 30 to 40° are observed. The mineral phase of low basicity BOF slag has been much less thoroughly investigated. Therefore, the references for the diffraction patterns are scarce to compare with this study. Qian et-al.$^{(3)}$ reported that the dominant phase in EAF slag with low basicity (CaO/SiO_2= 1.15) was kirschsteinite ($CaFeSiO_4$ structure). However, the XRD spectra in Fig. 2 and Fig. 3 are not consistent with their results of the X-ray diffraction pattern of kirschsteinite. The wustite phase is the only identified mutual phase in existence of all slags by the XRD spectra. Wustite is a major component of low basicity slag, being associated with its high peak height intensity, as shown in Figs. 2 and 3.

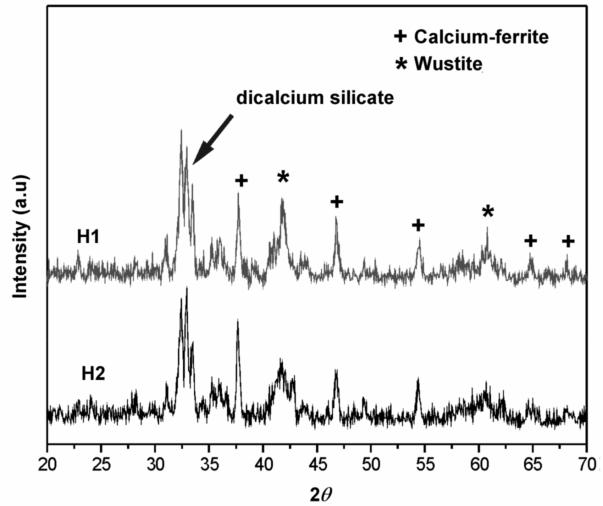

Fig. 1. X-ray diffraction pattern of slag samples: H1 and H2.

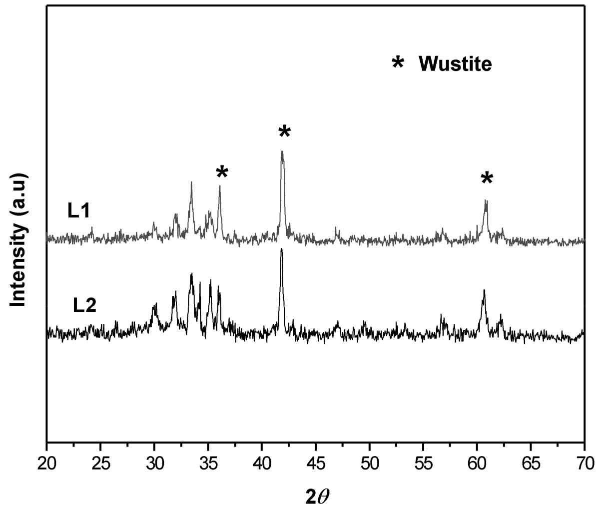

Fig. 2. X-ray diffraction pattern of slag samples: L1 and L2.

Table 1 Chemical Composition of BOF Slag Samples

No.	CaO	MgO	Al_2O_3	SiO_2	TiO_2	T-Fe	MnO	P_2O_5	CaO/SiO_2
	(wt %)								
H1	45.04	11.40	0.78	11.71	0.59	19.72	4.95	2.23	3.85
H2	46.09	10.05	0.84	12.80	0.57	19.27	4.92	2.34	3.60
L1	26.02	3.02	0.73	18.36	2.14	36.69	4.09	2.77	1.42
L2	27.98	2.36	0.76	21.85	1.120	28.79	10.04	4.10	1.28
L3	36.71	4.06	1.63	21.38	1.29	20.31	7.90	3.92	1.72
L4	34.25	2.56	1.58	19.88	1.02	26.30	8.05	3.00	1.72

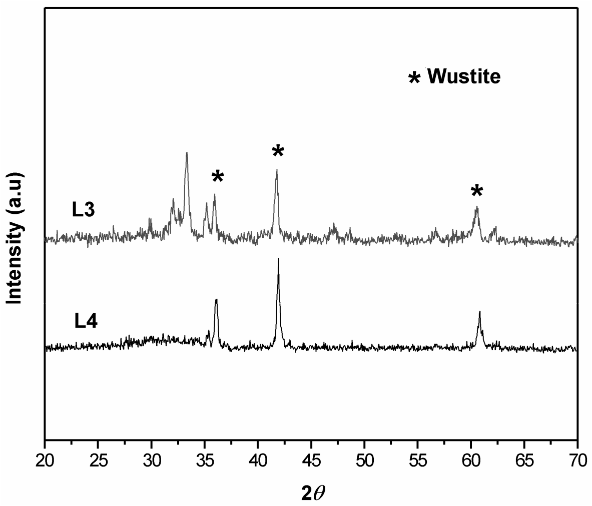

Fig. 3. X-ray diffraction pattern of slag samples: L3 and L4.

3.2 EPMA Analysis

(1) Slag with High Basicity

The mineral phases of dicalcium silicate (C_2S), calcium ferrite and wustite have been identified from the XRD results. Each mineral phase with specific feature morphology is shown in Fig. 4. The slag structures in Fig. 4 (a) mainly consist three mineral phases: the dark grain C_2S phase with a flat morphology; the calcium ferrite phase in gray color; and the magnesium-wustite phase with a bulge morphology. The white grains are identified as wustite in solid solution, as shown in Fig. 4 (b). Figure 5 illustrates the micrograph and composition as a function of the different phases of sample H1. With the dashed line representing the scanning positions, from the left to right are the magnesium-wustite, dicalcium silicate and calcium ferrite phases, respectively. The composition of the different phases can be distinguished with elemental content profile analysis. Phosphorus is concentrated in the scanning positions of the C_2S phase. The X-ray mapping of elements Mg, Si, P, Ca and Fe of the H2 sample is shown in Fig. 6. The distribution of the Ca element covers most of the mineral phase positions due to the high CaO concentration in high basicity slag. The mapping plot also indicates that P is incorporated in the C_2S phases.

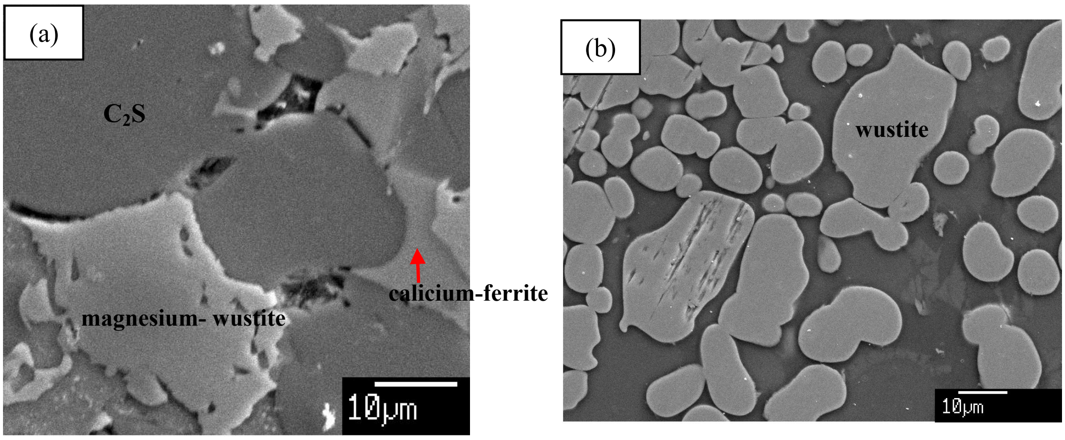

Fig. 4. Micrograph of different phases.

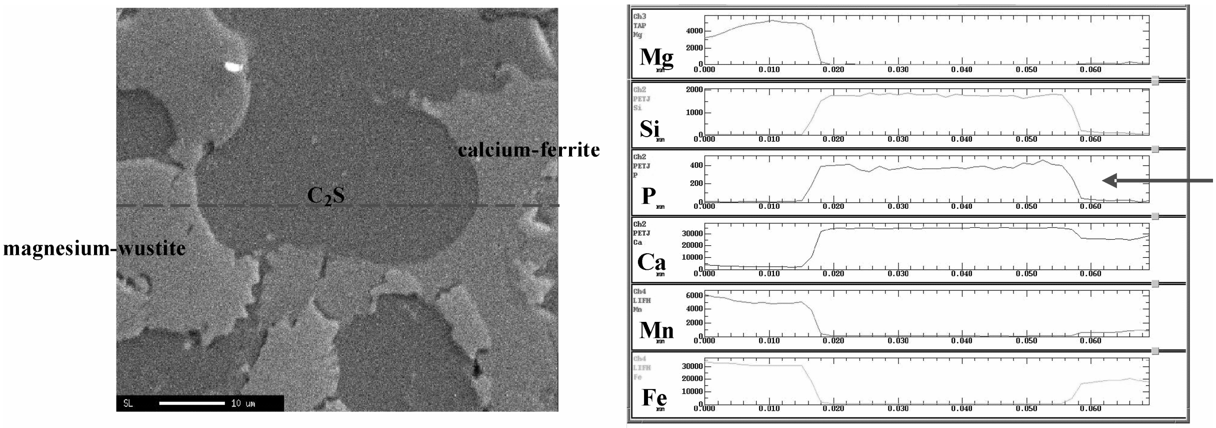

Fig. 5. Micrograph and composition as a function of different phases of sample H1.

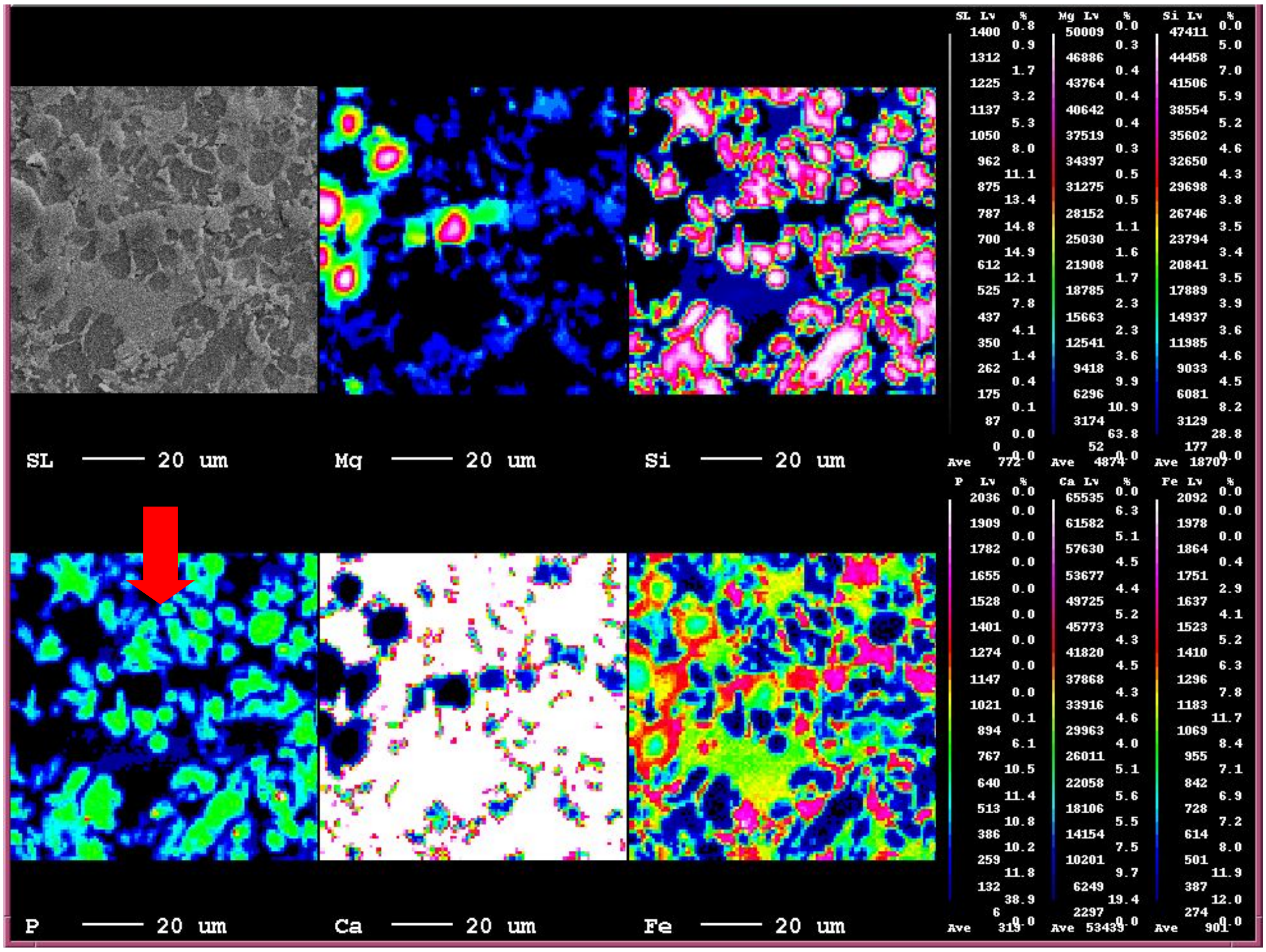

Fig. 6. Micrograph of H2 slag and EPMA mapping image of Ca, Si, Fe, Mg and P.

(2) Slag with Low Basicity

The morphologies are apparently different between high- and low basicity slag. The micrograph in Fig. 7 is obtained for slag sample L4, and the spot analysis of the marked positions is listed in Table 2. In Fig. 7, the wustite phase presents a dendritic structure, while the matrix consists of Ca, Fe, and Si oxide mineral phases. The composition of the matrix structure has a high percentage of CaO, and a nearly equal percentage of FeO and SiO_2 from the spot analysis in Table 2. The chemical composition and morphology of the matrix are appreciably different to the C_2S phase in high basicity. The X-ray mapping of elements Mg, Si, P, Ca, Al, O and Fe of the L4 sample is depicted in Fig. 8. Phosphorus is mainly bonded into a $CaFeSiO_4$ structure (uncertain stoichiometrically of $CaO{\cdot}FeO{\cdot}SiO_2$ composition is designated as $CaFeSiO_4$) which is outside the wustite phase. Figure. 9 shows the micrograph of slag sample L1, in which the spot analysis of the marked position is listed in Table 3. The white granular or dendritic structure is wustite. The P content is also concentrated in the $CaFeSiO_4$ structure.

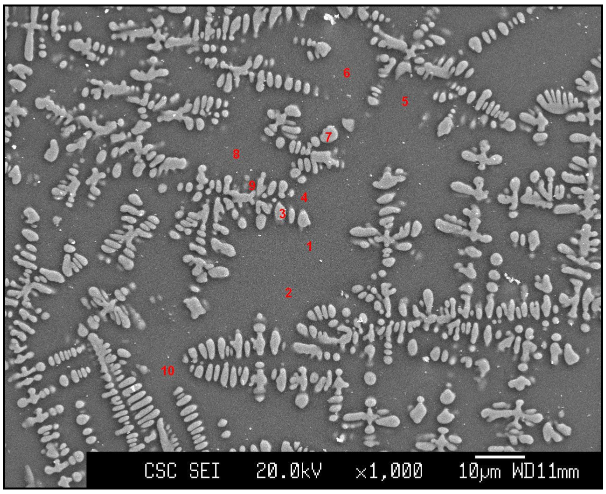

Fig. 7. Micrograph of L4 slag.

The wustite phase and $CaFeSiO_4$ structure are characterized in low basicity slag by EPMA analysis. In comparsion with the XRD results, the wustite phase is

Table 2 Composition of Spot Analysis in the Marked Positions Shown in Fig. 7

No.	CaO	MgO	SiO_2	FeO	MnO	P_2O_5
	(wt %)					
1	35.86	2.59	27.92	25.49	3.75	3.57
2	36.28	2.61	27.26	26.06	3.40	3.55
3	2.92	2.41	2.08	88.29	3.93	0.24
4	31.89	2.87	25.08	32.06	3.81	3.54
5	37.06	2.68	28.80	23.19	3.66	3.81
6	37.21	2.61	27.40	24.68	3.61	3.67
7	2.47	2.34	1.26	89.74	3.93	0.15
8	37.17	2.60	29.25	22.74	3.62	3.81
9	29.09	2.47	23.76	37.46	3.89	2.75
10	36.96	2.57	28.71	23.44	3.80	3.69

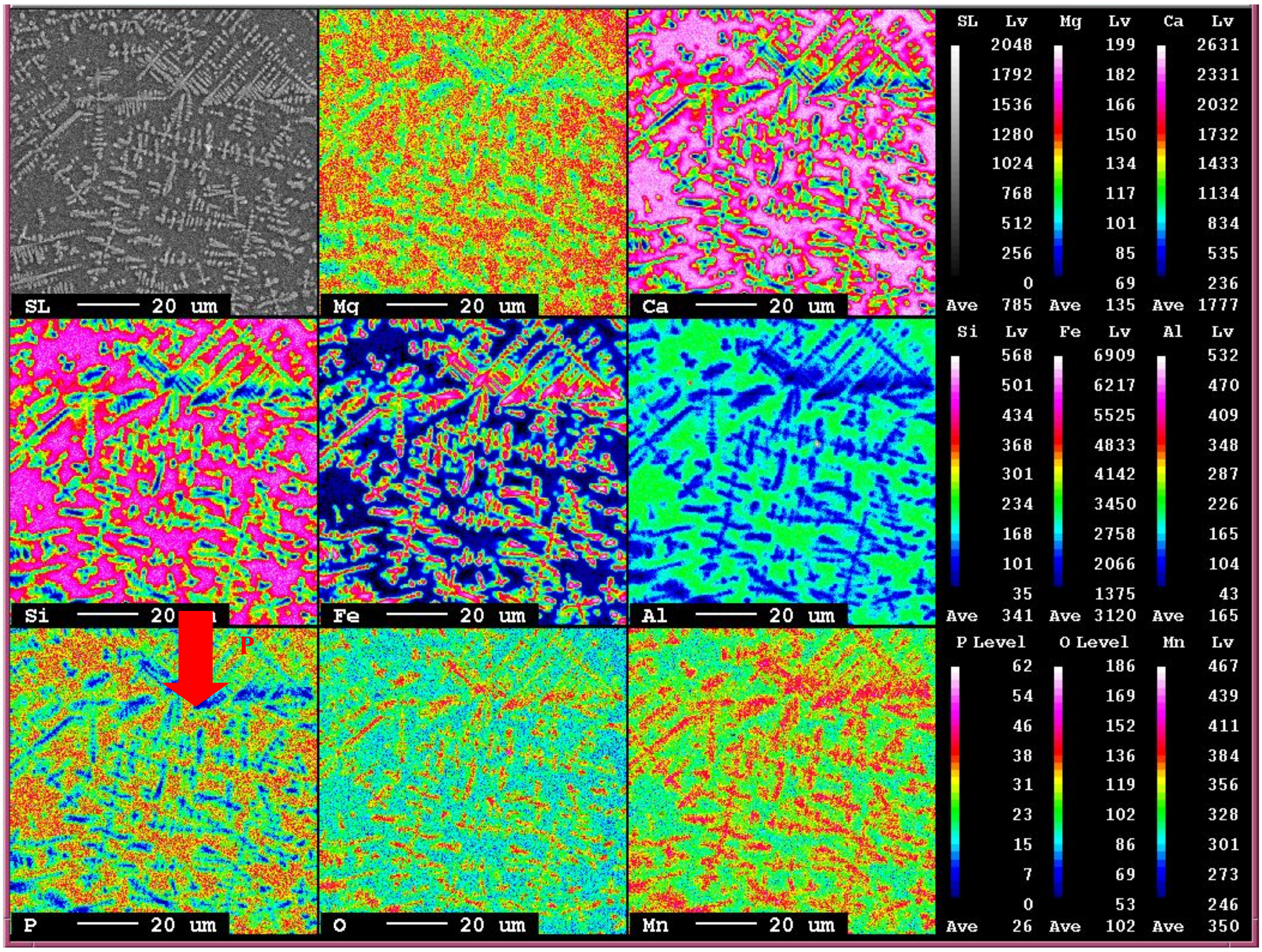

Fig. 8. Micrograph of L4 slag and EPMA mapping image of Ca, Si, Fe, Mg, Al, Mn, O and P.

Table 3 Composition of Spot Analysis in the Marked Positions Shown in Fig. 9

No.	CaO	MgO	SiO_2	FeO	MnO	P_2O_5
	(wt %)					
1	54.60	3.72	18.68	16.82	2.74	3.16
2	7.78	3.11	3.25	80.38	4.78	0.57
3	55.06	2.02	19.29	16.44	3.10	3.73
4	54.39	2.12	20.48	16.08	3.06	2.92
5	58.40	3.20	20.01	12.47	2.50	3.10
6	2.20	3.50	0.39	88.70	5.01	0.06
7	57.90	1.70	18.67	13.89	3.19	4.30
8	53.54	2.46	21.20	16.03	3.10	3.09
9	3.00	3.44	0.73	87.51	5.16	0.02
10	60.15	2.41	18.33	11.77	2.56	4.55

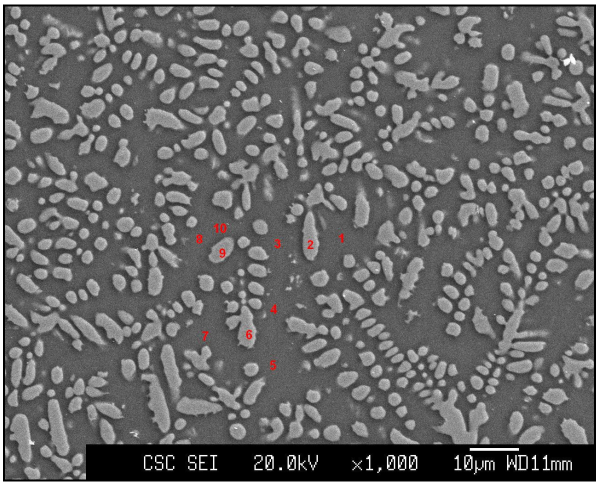

Fig. 9. Micrograph of L1 slag.

also the only identified mutual phase in all low basicity slags. Because of the variations in concentration of the CaO, SiO_2, and FeO components, the $CaFeSiO_4$ structure obviously depends on different slag samples from the spot analysis results. It is postulated that the $CaFeSiO_4$ structure was in existence during the different mineral phases with various compositions. Therefore, the XRD results in confirmation of the mutual mineral phases of the $CaFeSiO_4$ structure are not obtained in low basicity slag. However, phosphorus is bonded into a $CaFeSiO_4$ structure in all slag samples. More studies are required to clarify the mineral phase transformation of the $CaFeSiO_4$ structure in BOF slag with low basicity.

4. CONCLUSIONS

(1) Magnesium wustite, dicalcium silicate (C_2S), calcium ferrite and wustite phases are identified in BOF slag with high basicity, while wustite phase and $CaFeSiO_4$ structure are characterized in BOF slag with low basicity from the mineral phases examined either by XRD or by EPMA. However, a further study is needed to justify the mineral phases of the $CaFeSiO_4$ structure.

(2) The main phosphorous–containing mineral phases in BOF slag were C_2S with high basicity, and the $CaFeSiO_4$ structure with low basicity, respectively.

REFERENCES

1. Y. Ogawa, M. Yano, S. Kitamura and H. Hirata: Steel Research , 2003, vol. 74, No. 2, pp. 70-76.
2. R. Inoue and H. Suito: ISIJ, 1995, vol. 35, No. 3, pp. 272-279.
3. B. Deo, J. Halder, B. Snoeijer, A. Overbosch and R. Boom: Ironmaking and Steelmaking, 2005, vol. 32, pp. 54-60.
4. G. Qian, D. D. Sun, J. H. Tay, Z. Lai and G. Xu: Cem. Concr. Res., 2002 vol. 32, pp. 1377-1382.